Hindawi
Journal of Optimization
Volume 2023, Article ID 6682884, 20 pages
https://doi.org/10.1155/2023/6682884

Research Article

Optimization of Deformation Behaviors during Continuous Forming Extrusion of C18150 Copper Alloy through Response Surface Methodology

Tariku Desta, Devendra Kumar Sinha, and Perumalla Janaki Ramulu

Department of Mechanical Engineering, School of Mechanical, Chemical and Materials Engineering, Adama Science and Technology University, Adama, Ethiopia

Correspondence should be addressed to Perumalla Janaki Ramulu; perumalla.janaki@astu.edu.et

Received 3 June 2023; Revised 20 July 2023; Accepted 24 August 2023; Published 31 August 2023

Academic Editor: Himadri Majumder

Continuous extrusion (CE) is a method of creating endless profiles of high-quality products of dimensional accurateness, high productivity, and excellent material properties. The main objective of this study is to investigate the influence of CE input process parameters on optimal overall extrusion load requirement and effective stress induced. The input parameters considered were extrusion driving wheel speed, feed metal temperature, tool temperature, and factor of friction proceeding. Numerical simulations of a copper alloy (C18150) were carried out using DEFORM-3D to investigate the impact of the input variables on total load and effective stresses. A mathematical model based on response surface methodology (RSM) was developed for optimized results. The optimized parameters in terms of wheel extrusion velocities, feedstock temperatures, tool temperatures, and friction factors expressed. The ANOVA test was performed to assess the suitability and appropriateness of the model. Using RSM, the optimal load value of 408.167 kN and effective stress of 1241.0 MPa were achieved within the composite preference of 1.0. A load of 408.167 kN had been obtained if the velocity of the wheel, temperatures of feedstock, tool temperatures, and factors of friction are 4 rpm, 500°C, 400°C, and 0.85, respectively. The minimum effective stress of 1241.0 MPa is induced in the feedstock due to the CE process if the velocity of the wheel, temperature of the feedstock, die temperature, and frictional factor were 4 rpm, 500°C, 400°C, and 0.95, respectively.

1. Introduction

Demand for continuous product profiles for numerous engineering applications is expanding continuously. The primary constraint of the traditional extrusion process is that it can only form discrete aspects. It is known that an innumerable dimension of product offerings could be formed with higher dimensional accurateness, excellent mechanical properties, and metallurgical properties using the continuous forming process [1]. Figure 1 depicts the concept of a continuous forming extrusion method as well as the tooling utilized.

Kim et al. [3] studied an effect occurring within process factors/variables on the conform process and its process characteristics. The investigation was performed with the aid of the mathematical simulation software DEFORM-3D. A material flow behavior, strain effect, and temperature distributions were studied. Kim et al. [4] used upper bound advanced technologies to estimate the power needed for feedstock deformation of the material from feedstock entrance to die withdrawal. Under various frictional variables considerations, the process of flash creation in a continuous extrusion process (CEP) for copper feedstock materials was examined [5]. An analytical model was developed and investigated the mechanics of flash creation in a CEP. A functional connection was discovered among flash creation, pressure of extrusion, friction, and dimension of flash gap [6]. For the CEP, a mathematical model was made to predict stress, temperature, strain rate, and strain areas within the work material. Significant CEP process control and enhancement data were made available [7]. The material flow and processing parameters were

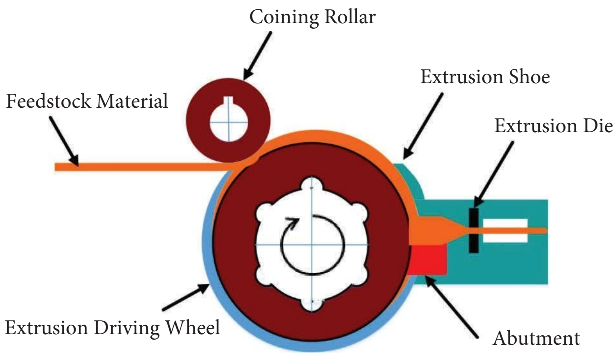

Figure 1: Schematic representation of the continuous extrusion method principle.

affected by changes in tool geometrical parameters in the CEP. It was recommended that tool designs be simplified [5]. To improve product quality and quantity, a control and sensing method was formed [8–10]. Analytical and mathematical studies were performed for the investigation of the surface defects and the curling circumstance [11–13]. The effect velocity of the wheel in the continuous extrusion process for examination effective stresses and strains, field of temperature, and damage were examined during CE manufacturing of *Cu* bars [14]. The optimized velocity of wheel amount for improving grain size and growth in a CEP for AA6063 feedstock materials were decided and discovered [15]. Sinha and Kumar et al. [16] developed prediction models of an optimized extrusion load utilizing different methods. The consequence temperature of feedstock in CEP was investigated in order to determine the optimum torque and load needed to extrude the material of feedstock thru the die orifice. The effects of CEP input parameters on extrudate microstructural and mechanical properties were investigated [17]. The mechanical belongings of continuously extruded rod of feedstock aluminum alloy, for instance, hardness and ultimate tensile strength, were optimized by optimizing process variables such as speed of wheel and ratio of extrusion [18]. The extrusion temperature of wheel, feedstock rod temperature, and extrusion wheel circumferential speed all have a major effect on the overall CEP [19–21]. Numerical models were developed and optimized CE process variables through RSM, artificial neural network (ANN), and genetic algorithm (GA). The numerical result was verified and in good agreement with the experimental one [22–26].

Many research studies have been performed in the continuous forming process (CFP) on copper and aluminum alloys, whereas a few research studies have been conducted on C18150 alloy for the evaluation and optimization of CEP parameters to determine their impacts on significant process attributes. As a result, in this study, the process variables in the CEP were optimized using RSM to figure out the minimal extrusion load demand for the extrusion of the raw material rod from of the entering of the feedstock rod into the groove portion of the wheel up to die ejection, as well as the minimum effective stress induced in the extrudate of C18150.

2. Materials and Methodology

Computational investigation, mathematical modeling, and optimization of CE process variables were performed to explore the effects of CE independent variables on extrusion load and effective stress during CE processing of C18150 feedstock material. The details of independent process variables with their respective levels and the experimental plan for C18150 are shown in Tables 1 and 2, respectively. The four input variables such as wheel speed, feedstock temperature, die temperature, and friction factor of the CE process were investigated for their effect on responses such as extrusion load and effective stress. The independent variables at three levels were taken into consideration, and homogeneous variability in decision variables was taken. This decision aided in comprehending how parameter levels influence responses. Simulation preprocess conditions were performed as per Table 3. The summary of tetrahedral mesh elements is also shown in Table 4. Experiments were designed and planned on four factors and at three levels to optimize the experimental conditions using the RSM Box–Behnken design method through Minitab tool. For computational investigation, a C18150 alloy with 12.5 mm in diameter feedstock material was taken to manufacture an extrudate diameter of 8 mm. All numerical simulations were performed numerically through DEFORM-3D software.

These parameters were considered based on TBJ 350 conform extrusion machine technical specifications (RPM setup), feedstock hot working temperature for Cu alloys, and preliminary computational investigations [26–31].

Therefore, Table 2 displays a total of 27 experimentation plans developed to investigate an optimal extrusion load and effective stress during the CE processing of a C18150 feedstock material into an 8 mm diameter product diameter. The feedstock material's deformation investigation was carried out according to the experimental plan shown in Table 2.

For computational analysis of the alloy, necessary data such as geometry, simulation, and feedstock material data are presented in Table 3. For computational analysis through DEFORM-3D, the material and CEP toolings were designed with tetrahedral mesh elements. All toolings and feed metal were properly meshed to facilitate the analysis. So, because extrusion wheel is among the highest essential aspects, a very large mesh size is required. Table 4 summarizes the tetrahedral mesh elements [32, 33].

The results from the computational investigation further analyzed for optimal responses through RSM for finding out the minimum value of extrusion load and effective stress at a certain combination of the CE input variables. The parameters' influence and worthiness were evaluated using the analysis of variance (ANOVA) tool. Based on the *P* values ($P < 0.05$) of coefficients in the ANOVA table, the significance of the CE parameters were identified and mathematical modeling was developed taking second-order regression function in equation (equation (1)). The general regression mathematical model adopted for the total load necessary to extrude a C18150 alloy was expressed in equation (1). The equation was used for finding out

Table 1: Independent parameters and their levels for experimental plan for C18150.

Factors	Levels		
	−1	0	1
Wheel velocity (rpm)	4	8	12
Feedstock temperature	500	600	700
Die temperature	400	500	600
Friction factor	0.85	0.90	0.95

Table 2: Box–Behnken design of C18150 feed for a product diameter of 8 mm.

S. no	Wheel velocity (rpm)	Feedstock temperature (°C)	Die temperature (°C)	Friction factor
1	4	600	500	0.95
2	8	600	500	0.90
3	12	600	600	0.90
4	8	600	400	0.85
5	8	500	500	0.95
6	12	600	500	0.85
7	12	600	400	0.90
8	8	600	500	0.90
9	8	700	600	0.90
10	8	700	400	0.90
11	4	500	500	0.90
12	12	500	500	0.90
13	12	600	500	0.95
14	4	600	400	0.90
15	8	600	400	0.95
16	12	700	500	0.90
17	8	500	500	0.85
18	8	600	600	0.85
19	4	700	500	0.90
20	4	600	600	0.90
21	8	600	600	0.95
22	8	600	500	0.90
23	8	700	500	0.95
24	8	700	500	0.85
25	8	500	600	0.90
26	4	600	500	0.85
27	8	500	400	0.90

Table 3: Variables for simulation 12.5 mm C18150 feedstock.

S. no	Variables	Details
Data of geometry		
1	Diameter of wheel r, D (mm)	350
2	Die diameter, d (mm)	6
3	Flash-gap size, G (mm)	1
4	Die length, L (mm)	10
Data of simulation		
1	Velocity of wheel, N (rpm)	4, 8, 12
2	Initial temperature (°C)	20
3	Environment temperature (°C)	20
4	Die temperature (°C)	400–600

Table 3: Continued.

S. no	Variables	Details
Feedstock material data		
	Material	C18150
1	Yielding stress (MPa)	432.01
2	Tensile strength (MPa)	452.03
3	Sensitivity of strain rate	0.22
4	Capacity of heat (N/mm^{2}°C)	2.3
5	Conductivity (N/s°C)	238
6	Convection coefficient (N/s°C mm)	0.02
7	Emissivity	0.3
8	Boltzmann constant (N/s°C mm^{4})	5.669×10^{-11}
9	Interface heat transfer coefficient (N/s°Cmm)	30
10	Interface coefficient of friction	0.95 (wheel groove and feedstock), 0.03 (feedstock and shoe/abutment), and 0.05 (feedstock and die)

Table 4: Mesh element list summary.

S. no	Objects	Mesh elements
1	Workpiece	71,719
2	Extrusion wheel	148,537
3	Extrusion shoe	24,885
4	Coining wheel	65,307
5	Abutment	76,391
6	Die	45,589

a relationship between input process parameters and the response variables of the continuous extrusion process. The optimum values occurring due to the input variables were determined using RSM to predict the best output response variables (extrusion load and effective stresses) in the continuous extrusion forming process [32, 33].

The polynomial response of second-order mathematical model thought of as

$$Y_u = A + \sum b_i x_{\mathrm{iu}} + \sum b_{\mathrm{ii}} x^2_{\mathrm{iu}} + \sum b_{\mathrm{ij}} x_{\mathrm{iu}} x_{\mathrm{ju}}. \tag{1}$$

Equation (1) can be also explained in an elaborative manner in the following equation:

$$\begin{aligned} Y_u = {} & A + \mathrm{ax}_1 + \mathrm{bx}_2 + \mathrm{cx}_3 + \mathrm{dx}_4 + \mathrm{ex}_1{}^2 + \mathrm{fx}_2{}^2 + \mathrm{gx}_3{}^2 + \mathrm{hx}_4{}^2 \\ & + \mathrm{hx}_1 x_2 + \mathrm{jx}_1 x_3 + \mathrm{kx}_1 x_4 + \mathrm{lx}_2 x_3 + \mathrm{mx}_2 x_4 + \mathrm{nx}_3 x_4, \end{aligned} \tag{2}$$

where Y_u is the corresponding response; X_{iu} is the coded values of the i-th continuous extrusion parameters for the u-th experiments; and a, b, c, d, ..., b_i, b_{ii}, and b_{ij} are regression coefficients. The linear effect has nomenclature through the second term under the concatenation sign of this polynomial function, whereas the higher-order influence is represented by the third term.

3. Results and Discussion

3.1. Modeling and Optimization of Conform Processing of C18150 Alloy. The entire designed experiments (27) had all been computationally carried out using the finite element simulation platform DEFORM-3D. Each experiment represents the experimental strategy as well as the responses during the extrusion of the feed metal from its entrance into the grooved segment of the extrusion wheel to the completed deformation through the die discharge. The responses such as extrusion load and effective stress for each experimental run are presented in Table 5. Figures 2 to 4 show the total load prediction during CE processing of the C18150 feedstock material in the x-, y-, and z-directions, respectively. During investigation, the driving wheel was assumed as a rigid punch and a frictionless side plate [4]. The figures show that the load needed for extrusion rises originally as the feedstock material moves through the grooved part of the wheel, peaks whenever the feed material was about to be extruded in the die chamber, and finally reduces once the extrusion has taken place.

Figures 2 to 4 show the load distribution in the x-, y-, and z-directions, respectively, through feedstock material extrusion. The figures show that the load needed for extrusion rises originally as that of the feedstock material movements through into the grooved part of the wheel, peaks whenever the material is about to be extruded in the die chamber, and reduces once the extrusion has occurred.

3.2. Total Load Modeling to Conform Processing of a C18150 Alloy. Table 5 shows the computational results of the outcome parameters investigated during the manufacturing of an extrudate of a C18150 alloy. The table shows how the CE variables have an enormous impact on the outcome parameters investigated: the extrusion load and effective stress. The total load requirement analyzed to work within compliance with the research setup at numerous different working conditions such as wheel velocities, friction factors, and feedstock temperatures and die temperatures taking at a product diameter of 8 mm.

Taking the results of the load response, a mathematical model for the total load had been generated necessary to extrude a C18150 alloy considering the four input factors. The P values in Table 6 clearly demonstrate that the linear, the quadratic, and the interaction influences of input parameters significantly contributed to the regression function equation (2) since their own P values are less than 0.05. Therefore, the treatment or effect had a considerable effect on the dependent factor, which is extrusion load.

Table 5: Deform 3D simulation analysis results of C18150 alloy.

Exp. trail	x_1	x_2	x_3	x_4	Total load	Effective stress
1	4	600	500	0.95	799	1356
2	8	600	500	0.90	728	1391
3	12	600	600	0.90	766	1416
5	8	600	400	0.85	832	1413
5	8	500	500	0.95	929	1424
6	12	600	500	0.85	771	1398
7	12	600	400	0.90	786	1321
8	8	600	500	0.90	758	1369
9	8	700	600	0.90	802	1451
10	8	700	400	0.90	593	1401
11	4	500	500	0.90	696	1406
12	12	500	500	0.90	713	1431
13	12	600	500	0.95	657	1479
14	4	600	400	0.90	687	1354
15	8	600	400	0.95	771	1398
16	12	700	500	0.90	742	1384
17	8	500	500	0.85	692	1448
18	8	600	600	0.85	707	1406
19	4	700	500	0.90	744	1353
20	4	600	600	0.90	726	1424
21	8	600	600	0.95	629	1414
22	8	600	500	0.90	773	1439
23	8	700	500	0.95	749	1409
24	8	700	500	0.85	771	1398
25	8	500	600	0.90	605	1498
26	4	600	500	0.85	832	1355
27	8	500	400	0.90	680	1432

Note. The product diameter taken for computational simulation was 8 mm. x_1: wheel velocity; x_2: feedstock temperature; x_3: die temperature; and x_4: friction factor.

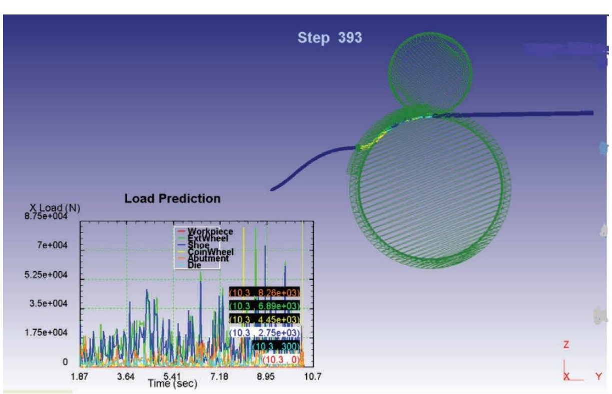

Figure 2: X-load distribution on a 12.5 mm C18150 alloy feedstock material.

Table 6 shows the vital considerable of factors impacting the dependent variable. Based on equation (2), the CE extrusion load during processing of C18150 feedstock is influenced by the extrudate diameter or extrusion ratio. The load amount needed during the process is also influenced by the feedstock and die temperatures. If the die and feedstock temperature levels are raised, the material's shear resistance decreases, lowering the load demand. The actual mathematical model was developed based on utilizing the data amount occurring in the coefficients revealed trendy Table 6 and is also shown in equation (2). In this expression, all the main, quadratic, and interaction effects of the CONFORM extrusion input process parameters had been taken into consideration. The coefficient of correlation (R^2) and adjusted R^2 values are 92.49% and 91.03%, respectively,

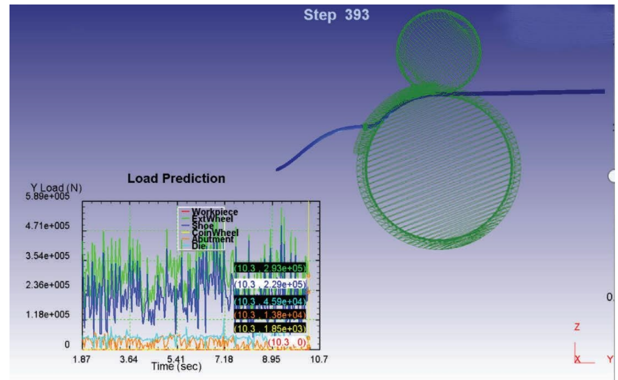

Figure 3: Y-load distribution of a 12.5 mm C18150 alloy feedstock material.

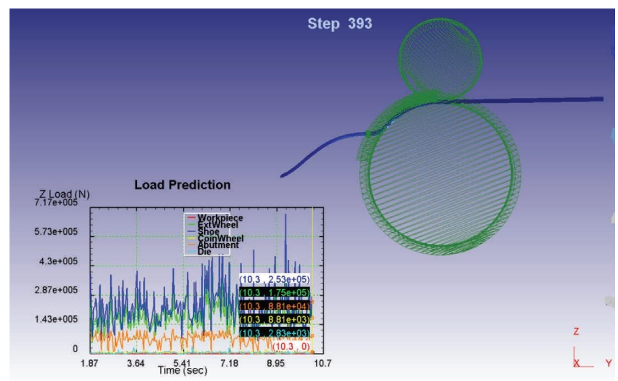

Figure 4: Z-load distribution of a 12.5 mm C18150 alloy feedstock material.

Table 6: Estimated regression coefficients for the extrusion load relevance/importance test for C18150.

Terms	Coefficients	Standard error coefficient	t-value	P value
Constant	8490.71	194.673	43.615	0.000
x_1	73.75	2.885	25.567	0.000
x_2	−8.22	0.124	−66.128	0.000
x_3	−23.80	0.121	−196.154	0.000
x_4	−310.00	372.869	−0.831	0.422
x_1^2	−2.31	0.031	−73.808	0.000
x_2^2	−0.00	0.000	−35.159	0.000
x_3^2	0.00	0.000	2.743	0.018
x_4^2	−8000.00	200.520	−39.896	0.000
$x_1 * x_2$	0.01	0.001	9.933	0.000
$x_1 * x_3$	0.15	0.001	104.085	0.000
$x_1 * x_4$	−126.25	2.894	−43.621	0.000
$x_2 * x_3$	0.00	0.000	64.783	0.000
$x_2 * x_4$	9.25	0.116	79.900	0.000
$x_3 * x_4$	22.55	0.116	194.782	0.000

x_1, wheel velocity; x_2, feedstock temperature; x_3, friction factor; x_4, die temperature.

Table 7: ANOVA to total load to extrude C18150 alloy.

Source	DoF	Sequential sum of square	Adjusted sum of square	Adjusted mean of square	F-value	P value
Regression	14	138933	138933	9923.8	7404.25	0.000
Linear	4	47200	61228	15307.1	11420.83	0.000
x_1	1	9577	876	876.1	653.66	0.000
x_2	1	56	5861	5860.9	4372.91	0.000
x_3	1	936	51569	51569.1	38476.41	0.000
x_4	1	36631	1	0.9	0.69	0.422
Square	4	9498	9498	2374.5	1771.68	0.000
x_1^2	1	5900	7301	7301.3	5447.63	0.000
x_2^2	1	1076	1657	1656.7	1236.12	0.000
x_3^2	1	388	10	10.1	7.52	0.018
x_4^2	1	2133	2133	2133.3	1591.71	0.000
Interaction	6	82234	82234	13705.7	10226.02	0.000
$x_1 * x_2$	1	132	132	132.3	98.67	0.000
$x_1 * x_3$	1	14520	14520	14520.3	10833.76	0.000
$x_1 * x_4$	1	2550	2550	2550.3	1902.78	0.000
$x_2 * x_3$	1	5625	5625	5625.0	4196.89	0.000
$x_2 * x_4$	1	8556	8556	8556.3	6383.94	0.000
$x_3 * x_4$	1	50850	50850	50850.2	37940.08	0.000
Residual error	12	16	16	1.3		
Lack-of-fit	10	16	16	1.6	*	*
Pure error	2	0	0	0.0		
Total	26	138949				

dof: degree of freedom.

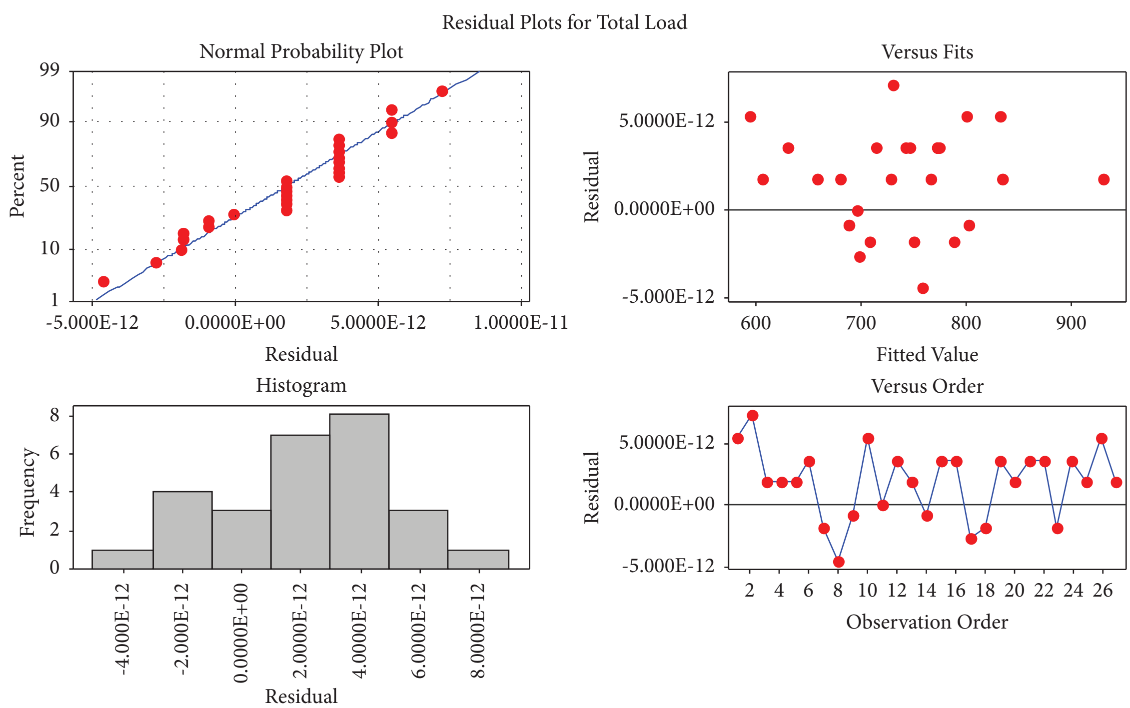

Figure 5: Residual plots for the total load.

indicating that the data are very well strongly associated with the produced regression mathematical model.

Based on the general regression mathematical model stated in the introduction section in equations (1) and (2), the actual mathematical model expression was developed for the total load. The model equation was constructed utilizing the coefficient values indicated within Table 6.

The actual mathematical model expression for the total load is

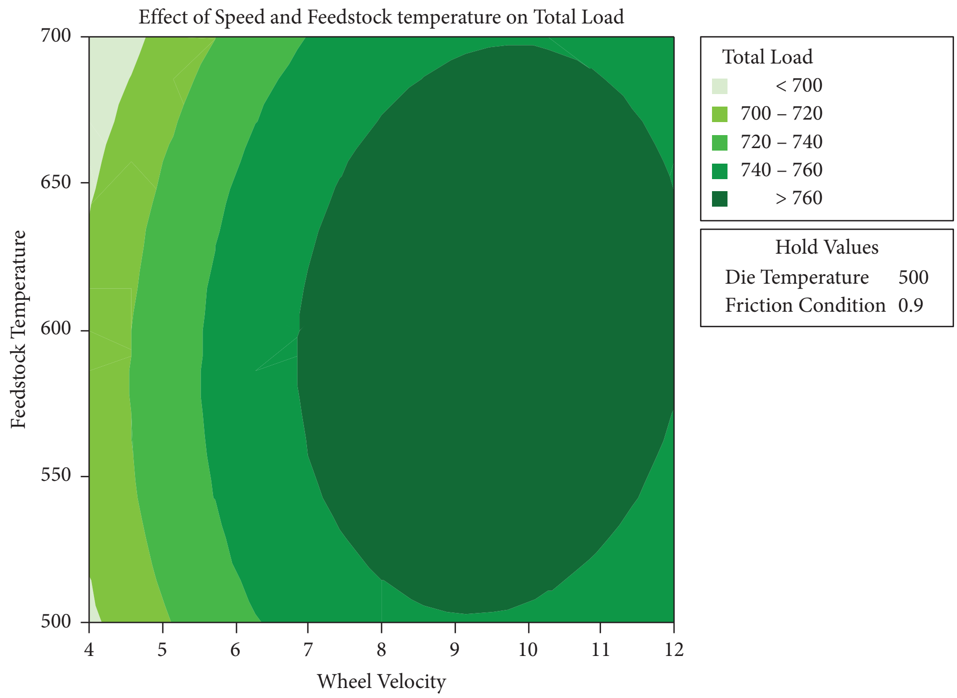

Figure 6: Influence speed of wheel and feedstock temperature to the total load.

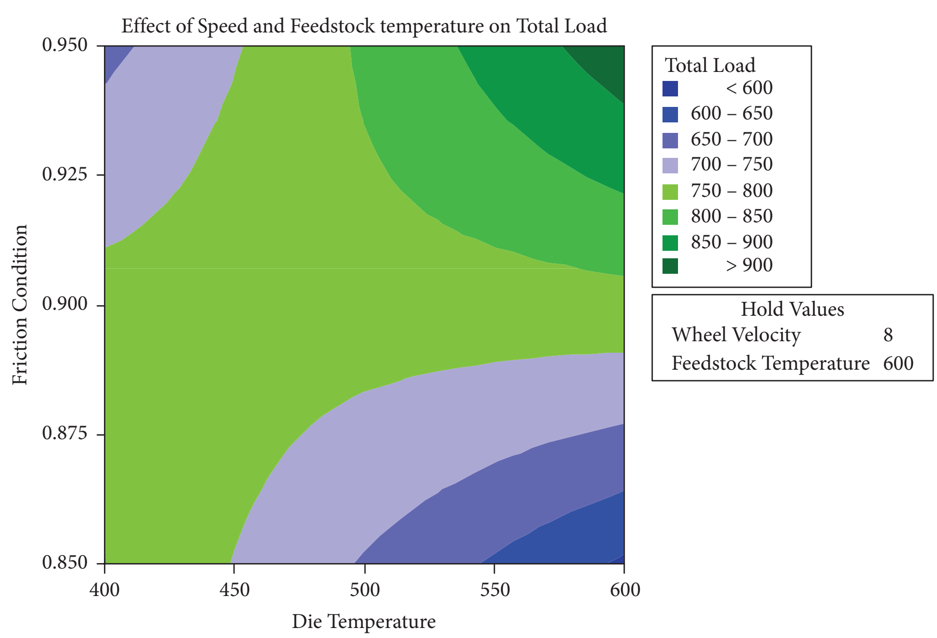

Figure 7: Effect temperature of die and factor of friction trendy the total/cumulative load.

$$\begin{aligned} Y = {} & 8490.71 + 73.75x_1 - 8.22x_2 - 23.80x_3 - 2.31x_1{}^2 \\ & - 8000x_4{}^2 + 0.01x_1x_2 + 0.15x_1x_3 \\ & - 126.25x_1x_4 + 9.25x_2x_4 + 22.55x_3x_4. \end{aligned} \quad (3)$$

Table 7 confirms that the F-values for all factors (main, linear, and quadratic effect velocity of wheel, factor of friction, feedstock and die temperatures, as well as the combined effect of item diameter and feedstock temperature and item diameter and die temperature) are much greater, indicating that the established mathematical model are statistically significant.

The influences of the parameters are also observed in Figure 5. The figure shows a residual graph for the dependent factor. It is evident that these residuals are normally distributed anywhere along the straight line and thus satisfy the circumstance of model fit. All the data points are very close to a straight line in the figure. The main influences are

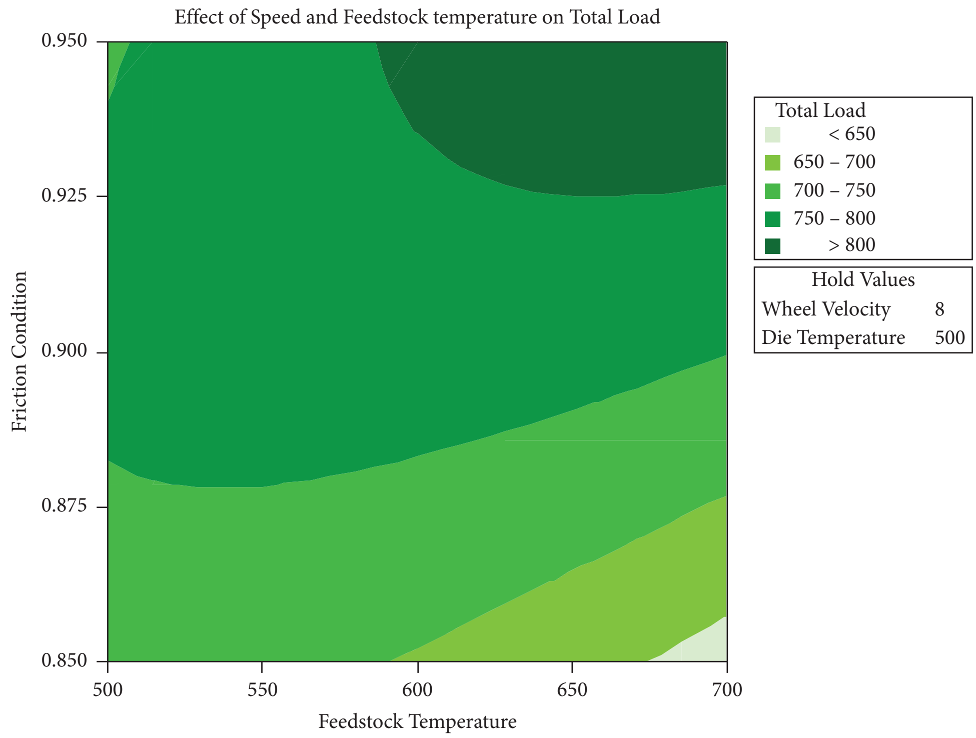

Figure 8: Effect of friction factor and feedstock temperature on the extrusion load.

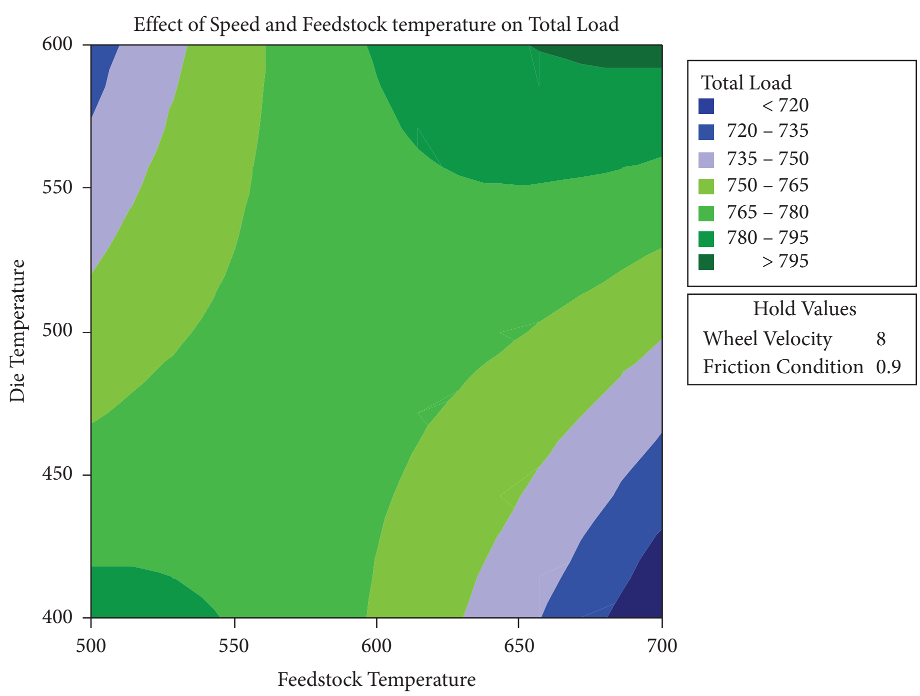

Figure 9: Effect of temperatures of die and feedstock on CE load.

defined as data that deviate from the straight line. Outliers are excluded from the entire data.

Figures 6 to 11 show the interaction or parametric combination effects of input procedure/process factors on the load needed for the CE of C18150 feedstock material. Figures 12 to 18 indicate the surface and optimization graph for the parametric combination of input procedure/process factors disturbing and influencing the subtotal load needed for the extrusion.

The effect of wheel speed and feedstock temperature on total load is observed in Figure 6. The load needed to extrude the material is the highest in the dark green zone and lowest

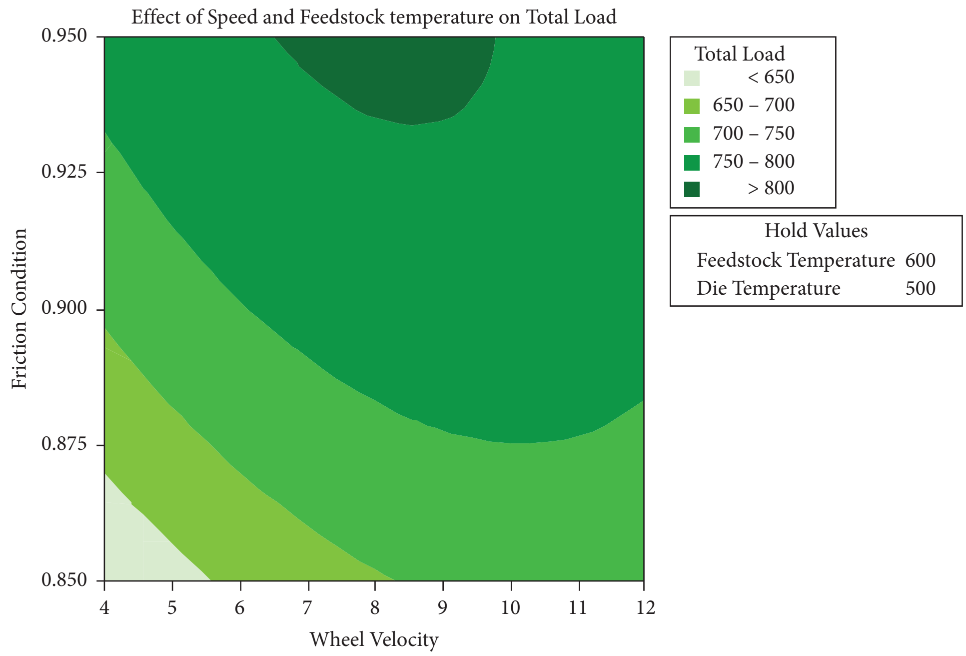

Figure 10: Effect of wheel speed and friction factor on the total load.

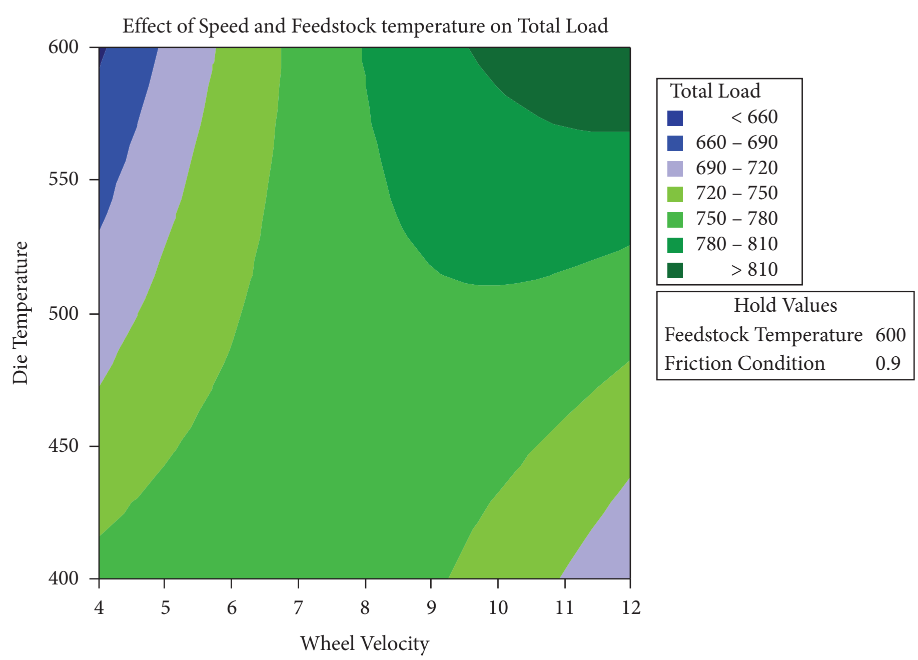

Figure 11: Effect of wheel speeds and die temperature on the deformation load.

in the light green zone. Based on the figure, less than 700 kN load is required for extrusion if wheel speed is set extremely low and feedstock temperature is set either very low around 500°C or very high above 640°C, taking holding values of the friction factor 0.9 and die temperature 500°C.

It is also observed the effect of die temperature and friction factor on the total load from Figure 7. A load required for extrusion of the alloy is maximum in the dark green zone and minimum in the dark blue zone. As a result, we could say that less than 600 kN extrusion load was required if the temperature of the die was set very high above 540°C and the friction factor was set below 0.865, holding values of wheel velocity at 8 rpm and feedstock temperature at 600°C.

It can also be perceived the effect temperature of feedstock and factor of friction on the total load from Figure 8. The load needed to alloy extrusion is greatest in the dark green zone and smallest within a light green zone. As a result, one can conclude that the least load required for the process was lower than 650 kN if the feedstock temperature

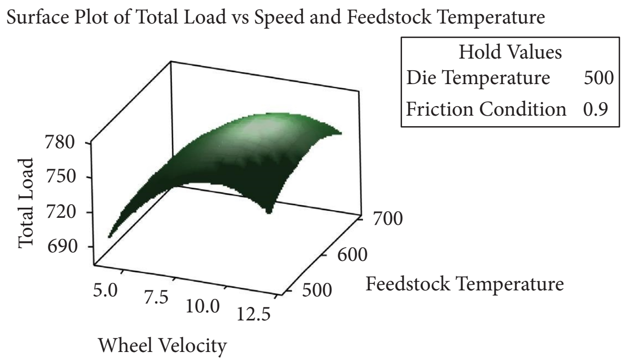

Figure 12: Surface plot of the total load vs. speed of wheel and temperature of feedstock.

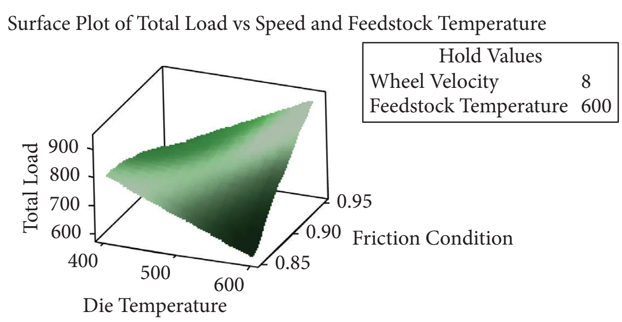

Figure 13: Surface graph occurred in total load vs. friction factor and die temperature.

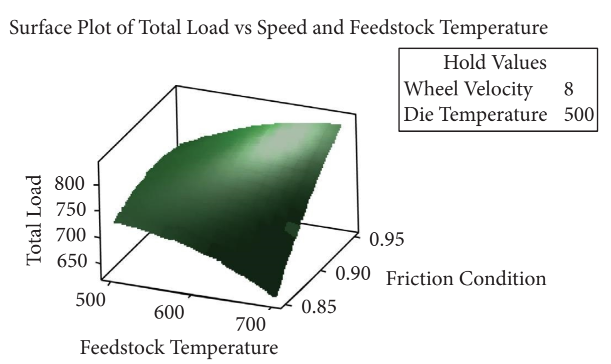

Figure 14: Surface graph occurred in total load vs. friction factor and temperature of feedstock.

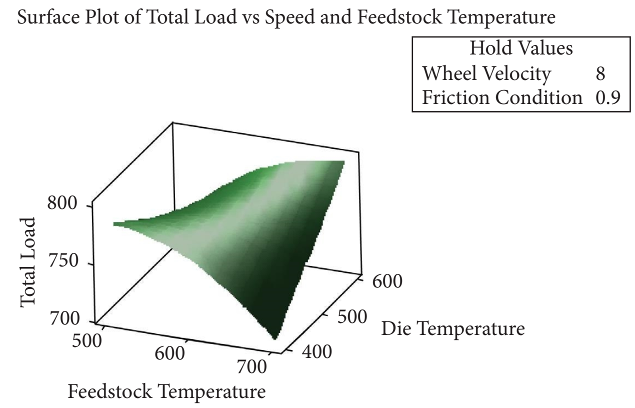

Figure 15: Surface graph occurred in total load vs. temperature of die and feedstock temperature.

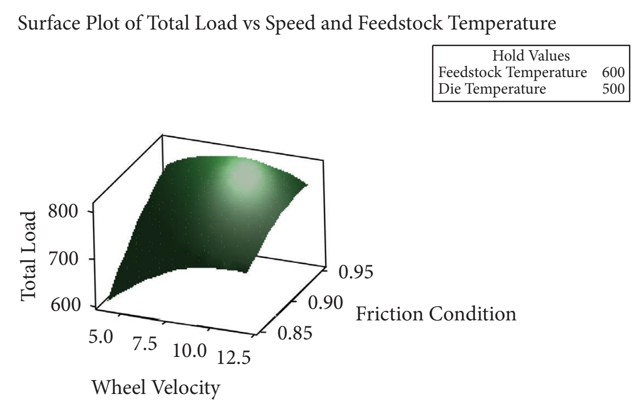

Figure 16: Surface graph occurred in total load vs. wheel speed and friction factor.

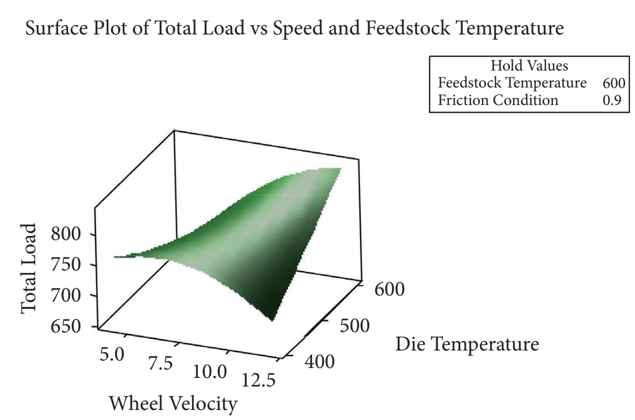

Figure 17: Surface plot of total load vs. wheel speed and die temperature.

was very high above 680°C and friction factor was very low below 0.865, holding wheel velocity at 8 rpm and die temperature at 500°C.

It can also be perceived on the effect of feedstock and die temperature the total load from Figure 9. The load needed for CE extrusion of C18150 alloy is greatest in the dark green zone and lowest in the dark blue zone. As a result, it is reasonable to conclude which the lowest load which is smaller than 720 kN can be applied for the CE extrusion of the alloy if the temperature occurring in the feedstock is above 680°C and temperature of die at around and just below 425°C, holding wheel velocity at 8 rpm and friction factor 0.9.

Also, the effect of wheel velocity and friction factor on the total load is seen from Figure 10. The load needed for material extrusion is greatest within the dark green zone and smallest inside the light green zone. Therefore, based on the graph, it is possible to get a load which is than 650 kN load applied for CE extrusion if both parameters such as wheel velocity and friction factor are very low level, taking holding

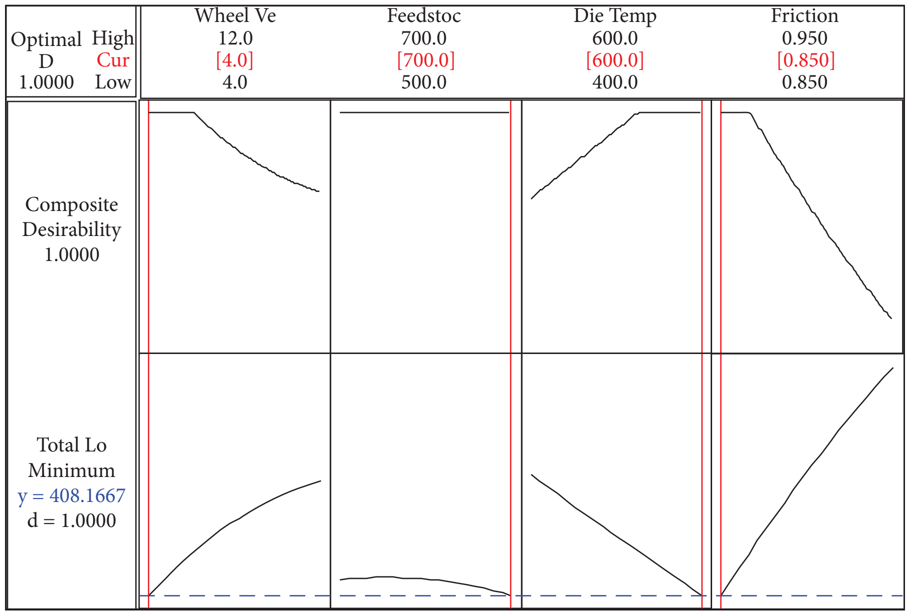

Figure 18: Optimization occurred in the total load effect of wheel speed, feedstock temperature, die temperature, and friction factor.

values of feedstock temperature at 600°C and die temperature at 500°C.

The influence of the wheel velocity and friction factor on extrusion load is apparent from Figure 11. The load needed to extrusion is the greatest in the dark green zone and least in the dark blue zone. Based on Figure 11, a load lower than 660 kN is required if the wheel velocity was very low around 4 rpm and die temperature was enormously high above 535°C with holding values of feedstock temperature at 600°C and friction factor 0.9.

Figure 12 shows a doom shape 3D surface plot of extrusion load response for wheel velocity and feedstock temperature variables. So, it is minimum if the input variables are set at their low levels simultaneously.

Figure 13 shows a flatted saddle-shaped extrusion load 3D surface plot for wheel velocity and die temperature variables. So, based on the plot, the CE extrusion load is least if the input variable of friction factor is low and die temperature is high at holding values of feedstock temperature of 600°C and wheel speed of 0.9.

Figure 14 shows a partially domed 3D surface plot of extrusion load for friction factor and feedstock temperature. So, the load is minima if the feed stock temperature is set at high and friction factor is low at holding values of 8 rpm for wheel speed and 500°C for die temperature.

Figure 15 shows a partially saddle 3D surface plot of extrusion load for feedstock temperature and die temperature. So, the load requirement is minimum if the former set at high and the latter at low taking holding values of 8 rpm for wheel velocity and 0.9 for friction factor.

Figure 16 shows a flattened and a bit offset doom looked 3D surface plot of load for wheel velocity and friction factor variables. So, the load is minimum if both variables set at their low levels simultaneously at holding values of FT of 600°C and DT of 500°C.

Figure 17 shows a flatted saddle-shaped extrusion load 3D surface plot for wheel velocity and die temperature variables. Thus, the lower load is required if the input variables are set at wheel velocity low and die temperature was high; or wheel velocity at high and die temperature is low at holding values of feed stock temperature of 600°C and friction facture of 0.9.

It is observed from Figure 18 that an optimized load of 408.167 kN is needed if the wheel velocity, feedstock and die temperatures, and frictional factor are 4 rpm, 700°C, 600°C, and 0.85, respectively. Utilizing RSM, the optimized load (408.167 kN) is achieved with something like the composite suitability and preferences of 1.0.

3.3. Modeling and Optimization of Effective Stress of a C181500 Alloy through RSM. A total of 27 numerical simulations were performed as per the experimental plan in Table 4. Computational experiments were carried out utilizing a finite element simulation platform DEFORM-3D to investigate the effects of the input variables on effective stress. Effective stress induced in the material was investigated according to the experimental setup at numerous different working conditions of velocities of wheel, friction factors, feedstock temperatures, and die temperatures shown in Table 4. The effects of continuous forming input process factors on effective stress were investigated, and the results of each simulation are indicated in Table 5. During a computational analysis of C18150 alloy using DEFORM-3D, the effective stress of the material considered encompasses all three stages. They are before the entry into the extrusion wheel's recessed part; during and after the CEP extrusion of the raw material through the die hole were considered. Table 5 also shows a computational result of the effective stress induced in the product upon CE processing of

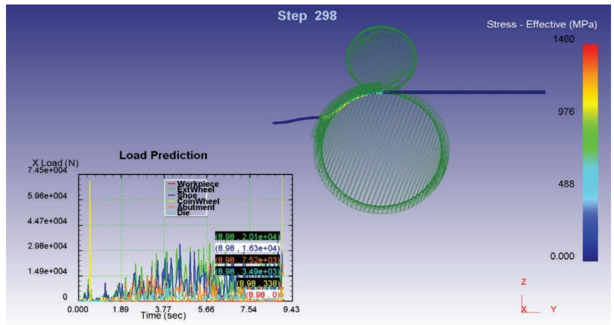

Figure 19: Effective stress distribution of a 12.5 mm Cu-Cr-Zr alloy material of feedstock.

Table 8: Estimated regression coefficients for effective stress (test of significance for extrusion effective stress for C18150).

Term	Coef	SE coef	T	P
Constant	11621.2	105.795	109.847	0.000
x_1	−67.2	1.568	−42.886	0.000
x_2	0.6	0.068	8.818	0.000
x_3	−1.4	0.066	−20.474	0.000
x_4	−21486.7	202.635	−106.036	0.000
x_1^2	1.7	0.017	99.108	0.000
x_2^2	−0.0	0.000	−64.695	0.000
x_3^2	−0.0	0.000	−43.589	0.000
x_4^2	8400.0	108.972	77.084	0.000
$x_1 * x_2$	−0.0	0.001	−0.795	0.442
$x_1 * x_3$	−0.1	0.001	−161.328	0.000
$x_1 * x_4$	112.5	1.573	71.525	0.000
$x_2 * x_3$	−0.0	0.000	−95.366	0.000
$x_2 * x_4$	3.5	0.063	55.630	0.000
$x_3 * x_4$	6.0	0.063	95.366	0.000

a 12.5 mm of C18150 feedstock to manufacture to an 8 mm extrudate.

Figure 19 displays an effective stress induced within the feedstock material due to the CE processes. It is observed from the figure that effective stress induced in a feedstock during the CE process rises at preliminary as that the material of feedstock keeps moving into the grooved segment of both wheels and reaches a highest whenever the material is in collision with the abutment and then it significantly reduces once extrusion has occurred.

Table 8 shows that the main, linear implications, the quadratic implications, and the interaction implications of input variables contributed significantly because their P values are higher than the least considerable value, 0.05. Based on the table, effective stress is reliant on input variables such as driving wheel velocity, feedstock temperature, friction factor, and die temperature. When the die and feedstock temperatures are raised, the material's shear resistance decreases, lowering the effective stress need during CEP. Optimized effective stress has a significant effect on power requirements and tool life [34].

The actual mathematical model is developed based on utilizing a data amount to the coefficients shown in Table 8 and revealed within equation (4). In the expression, all the main, quadratic, and interaction effects of the CE input process parameters are taken into consideration.

The F-value for the linear and quadratic impacts velocity of wheel, temperature of feedstock, temperature of die, factors of friction, the interaction outcome feedstock temperature, and die temperature seems to be indeed very considerable effect. Table 9 indicates that the established mathematical model was statistically significant.

Therefore, the developed mathematical model expression for the effective stress is

$$\begin{aligned} Y = {} & 11621.2 - 67.2x_1 + 0.6x_2 - 1.4x_3 - 21486.7x_4 + 1.7{x_1}^2 + 8400{x_4}^2 \\ & - 0.1x_1x_3 - 112.5x_1x_4 + 3.5x_2x_4 + 6.0x_3x_4. \end{aligned} \tag{4}$$

From RSM results, if P value of whatever treatment <0.05, the treatment has a considerable impact on the dependent variable, effective stress. Table 9 shows significant/vital factors influencing dependent factors. The coefficient of correlation (R^2) and adjusted R^2 values are 91.49% and 86.03%, respectively, indicating that

Table 9: ANOVA effective stress to extrude C18150 alloy.

Obs.	Std. order	Effective stresses	Fit	SE fit	Residual	Standard residuals	F-value	P value
1	16	1356.000	1355.833	0.481	0.167	0.41	7393.07	0.000
2	15	1391.000	1390.667	0.481	0.333	0.82	3566.56	0.000
3	11	1416.000	1416.333	0.481	−0.333	−0.82	1839.20	0.000
4	24	1413.000	1413.125	0.481	−0.125	−0.31	77.76	0.000
5	8	1424.000	1423.542	0.481	0.458	1.13	419.20	0.000
6	27	1398.000	1398.000	0.363	0.000	0.00	11243.65	0.000
7	13	1321.000	1321.167	0.481	−0.167	−0.41	7905.42	0.000
8	17	1369.000	1368.792	0.481	0.208	0.51	9822.32	0.000
9	5	1451.000	1450.708	0.481	0.292	0.72	4185.47	0.000
10	6	1401.000	1400.208	0.481	0.792	1.95	1900.00	0.000
11	1	1406.000	1405.708	0.481	0.292	0.72	5941.89	0.000
12	10	1431.000	1430.667	0.481	0.333	0.82	8737.89	0.000
13	19	1479.000	1479.792	0.481	−0.792	−1.95	0.63	0.442
14	7	1354.000	1354.042	0.481	−0.042	−0.10	26026.74	0.000
15	26	1398.000	1398.000	0.363	0.000	0.00	5115.79	0.000
16	2	1384.000	1383.875	0.481	0.125	0.31	9094.74	0.000
17	18	1448.000	1447.958	0.481	0.042	0.10	3094.74	0.000
18	14	1406.000	1406.333	0.481	−0.333	−0.82	9094.74	0.000
19	23	1353.000	1352.958	0.481	0.042	0.10		
20	21	1424.000	1424.625	0.481	−0.625	−1.54	*	*
21	22	1414.000	1414.792	0.481	−0.792	−1.95		
22	12	1439.000	1439.000	0.481	0.000	0.00		
23	4	1409.000	1408.542	0.481	0.458	1.13		
24	25	1398.000	1398.000	0.363	0.000	0.00		
25	9	1498.000	1498.000	0.481	0.000	0.00		
26	20	1355.000	1355.958	0.481	−0.958	−2.36 R		
27	3	1432.000	1431.375	0.481	0.625	1.54		

R denotes an observation with a large standardized residual.

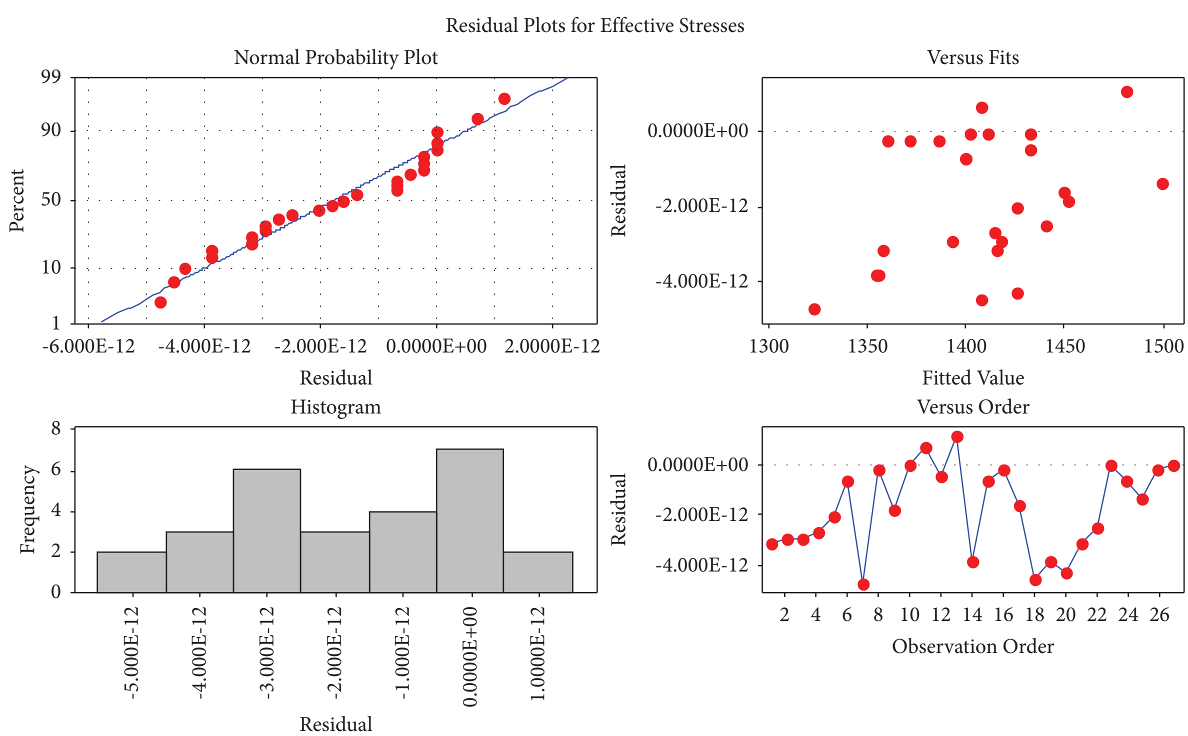

Figure 20: Residual plots for effective stress.

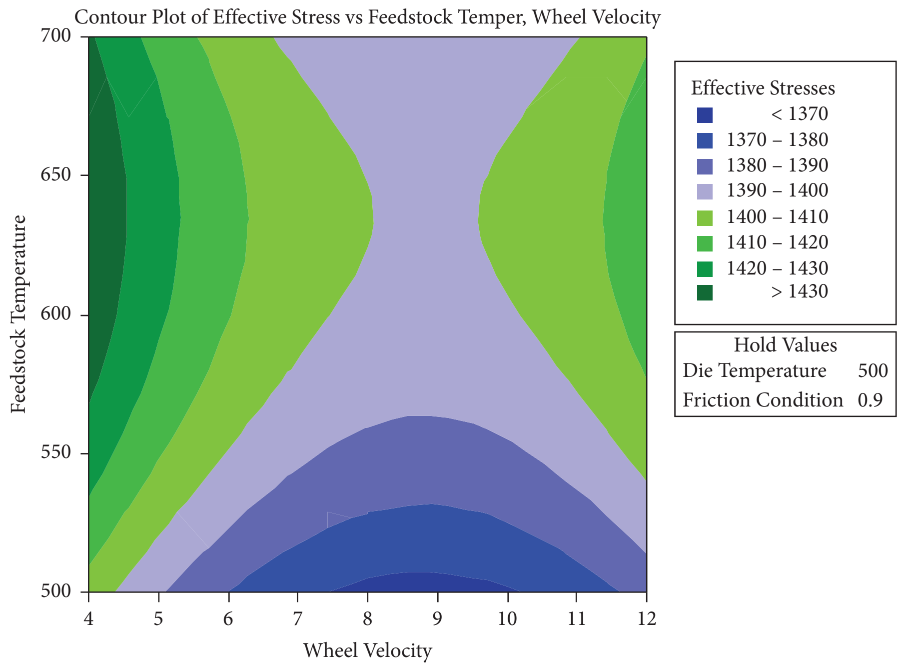

Figure 21: Effect of wheel speed and feedstock temperature on effective stress.

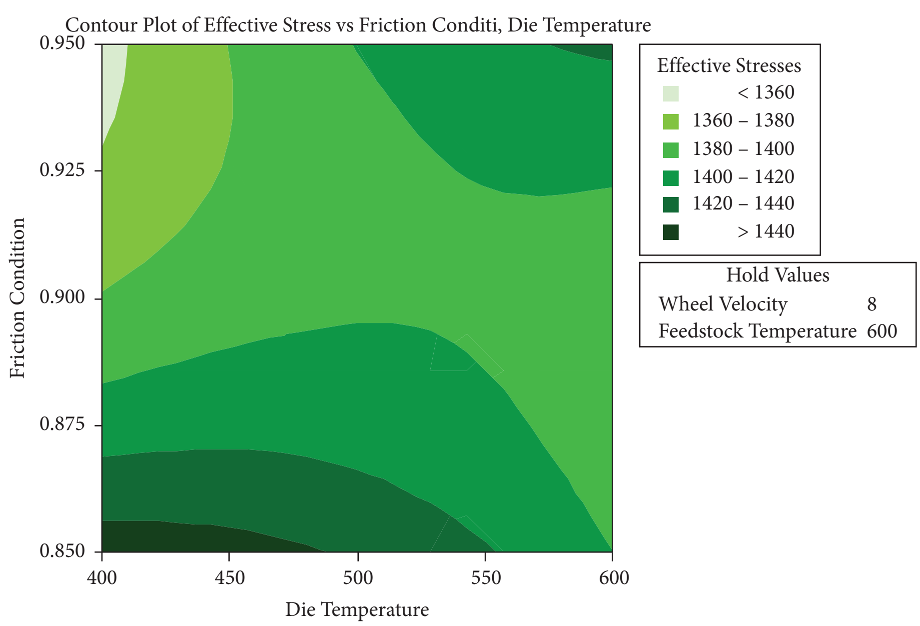

Figure 22: Effect of die temperature and friction factor on effective stress.

perhaps the data are very well strongly correlated with the produced regression mathematical model.

The F-value for the linear and quadratic impacts velocity of wheel, temperature of feedstock, temperature of die, factors of friction, the interaction outcome of item diameter, and feedstock temperature, and the interaction outcome of item diameter and die temperature seems to be indeed very considerably great within Table 9, indicating that the established mathematical model was statistically significant.

Figure 20 depicts the residual graph for the dependent factors, effective stress. The graph demonstrates that all residuals are homogeneously and nearly normally distributed all along the straight line, satisfying the circumstance of model fit. Figure 20 also shows that all of the data points are indeed very close to the straight line. Significant effects are defined as data that deviate from the straight line. Outliers are almost always eliminated first from rest of the data information.

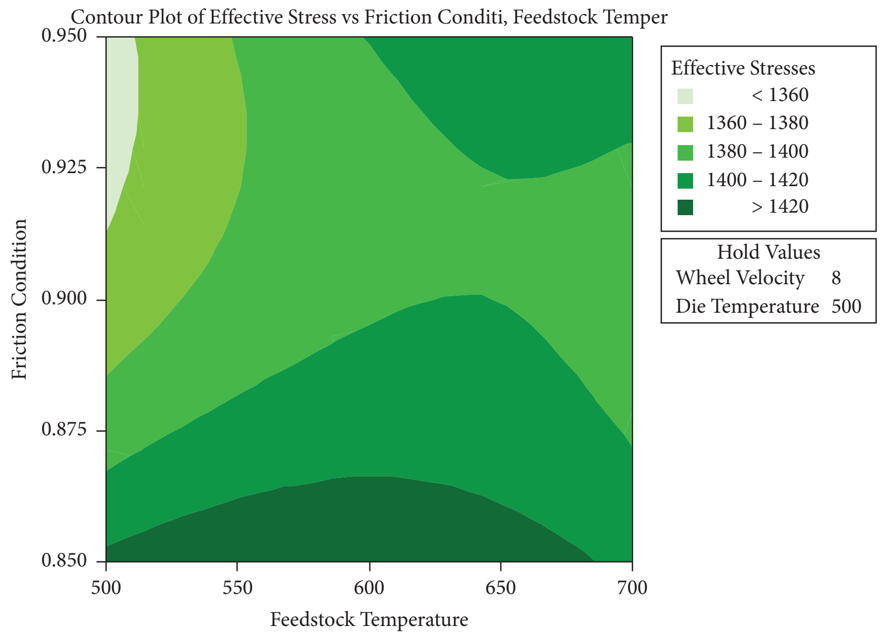

Figure 23: Effect of friction factor and feedstock temperature on effective stress.

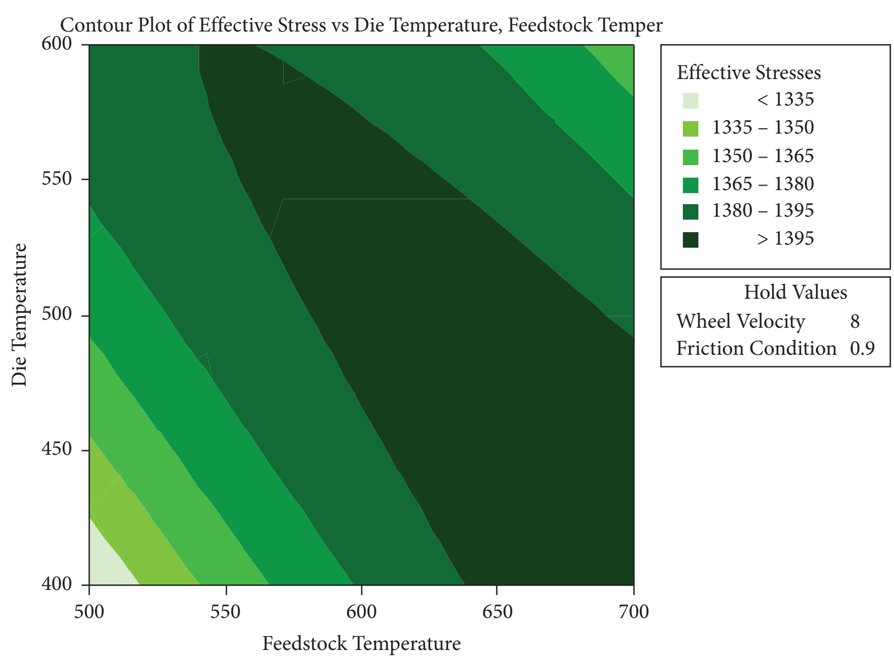

Figure 24: Effect of die temperature and feedstock temperature on effective stress.

From Figures 21 to 26, the parametric combination effects of input variables on effective stress induced in the material during the entire CE extrusion processing of C18150 alloy are shown; however, from Figures 27 to 33, surface plots and a graph of minimization were displayed for the interaction effects of CE input process variables on effective stress.

It is illustrated in Figure 21 that feedstock temperature and speed of the driving wheel have influence on effective stress induced in the material. During the entire CE extrusion processing of C18150 alloy, the stress induced in the alloy is the largest in the dark green zone and least in the dark blue zone. As a result, it is reasonable to determine that less than 1370 N/mm^2 effective stress was induced in the feed metal if the wheel speed is between 7.5 and 10.2 rpm and feedstock temperature is lower than 520°C at holding values of the friction factor 0.9 and the die temperature 500°C.

An effect of effective stress that occurred due to die temperature and friction factor is observed in Figure 22. The stress in the dark green zone is the greatest and the least in the light green zone. As a result, it was possible to deduce using the figure that less than 1360 N/mm^2 effective stress

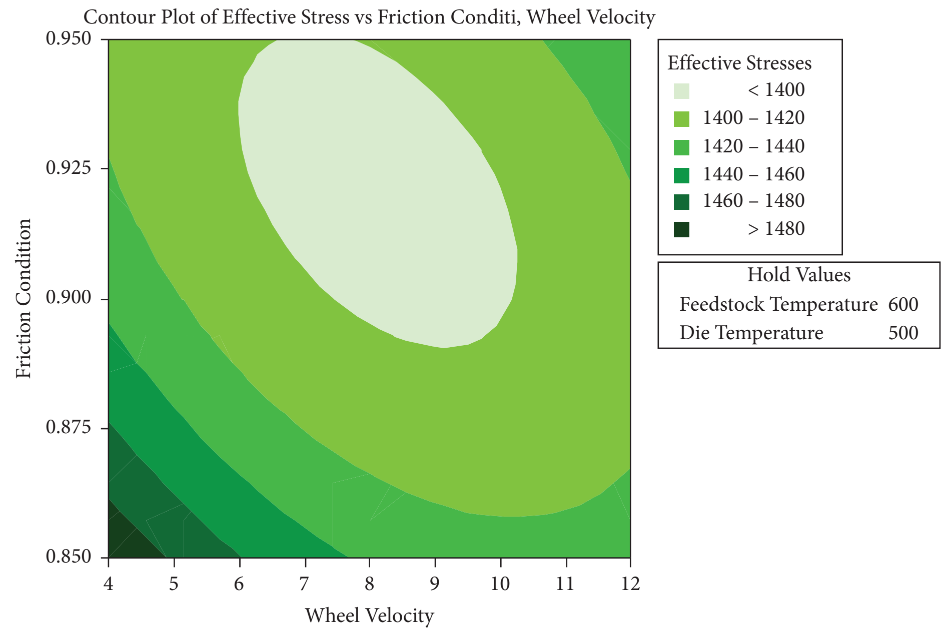

Figure 25: Effect of wheel speed and friction factor on effective stress.

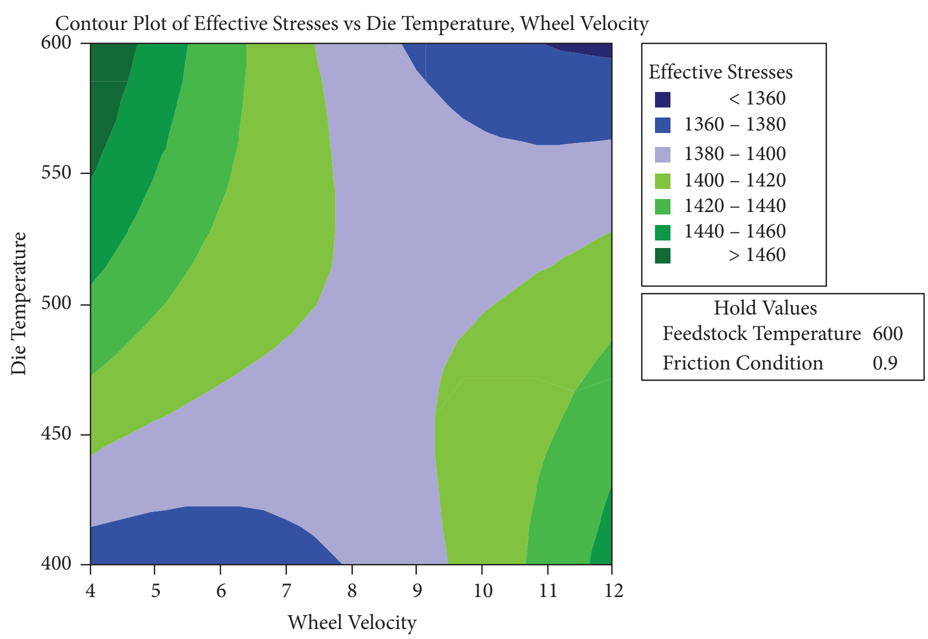

Figure 26: Effect of wheel speeds and die temperature on effective stress.

induced if the die temperature is less than 420°C, the friction factor is very high at holding amounts of velocity of wheel at 8 rpm and the temperature of feedstock at 600°C.

The effect of feedstock temperature and friction factor on effective stress is observed in Figure 23. It could also be perceived from the figure that the stress was maximum in the dark green zone and least in the light green zone. As a result, it is reasonable to infer from the figure that the least effective stress was induced in the CE process if the feedstock temperature is lower than 520°C and the friction factor was very high above 0.910 at holding amounts velocity of wheel at 8 rpm and temperature of die tat 500°C.

It can also be perceived the effect of feedstock and die temperatures on effective stress induced in Figure 24. The stress in the C18150 alloy is the greatest in the dark green zone; however, it was the least in the light green zone As a result, it is possible to deduce that lower than 1335 N/mm^2 effective stress is induced if both the feedstock and die temperature were of very low levels with holding velocity of the wheel at 8 rpm and friction factor at 0.9.

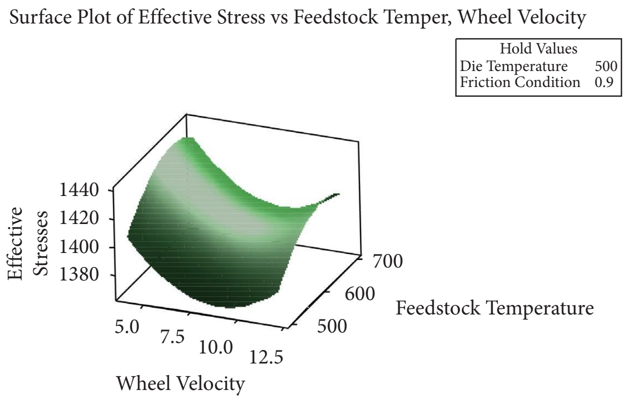

FIGURE 27: Surface graph occurred in effective stress vs. speed of wheel and temperature of feedstock.

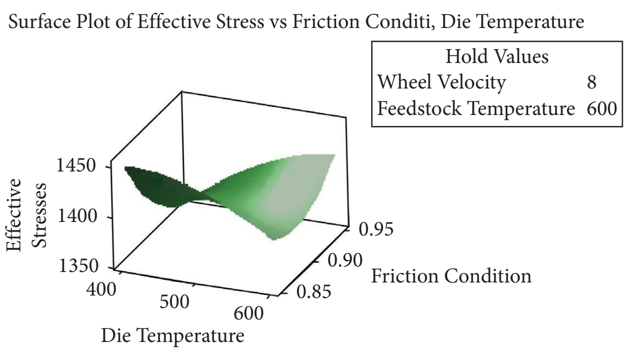

FIGURE 28: Surface graph occurred in effective stress vs. die temperature and friction factor.

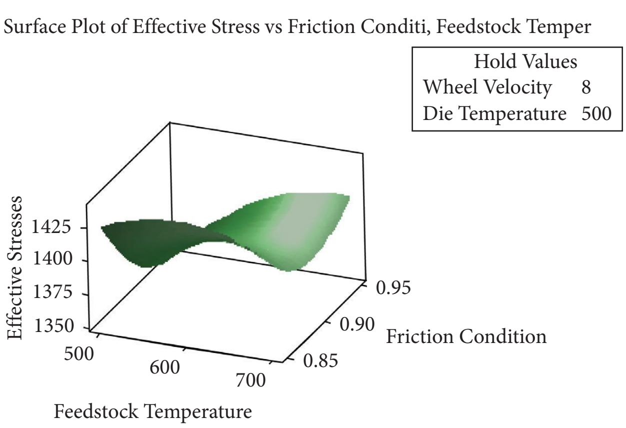

FIGURE 29: Surface graph occurred within effective stress vs. feedstock temperature and friction factor.

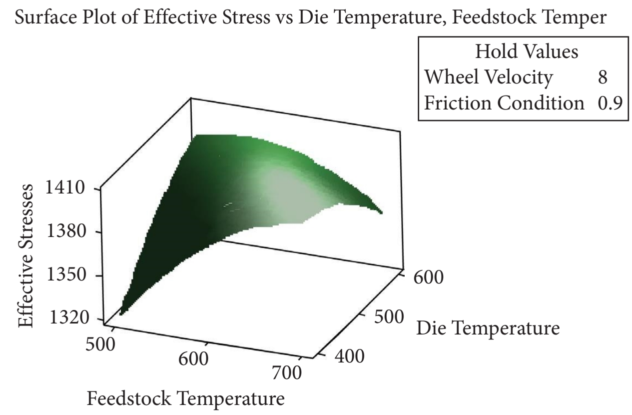

FIGURE 30: Surface graph occurred within effective stress vs. feedstock temperature and die temperature.

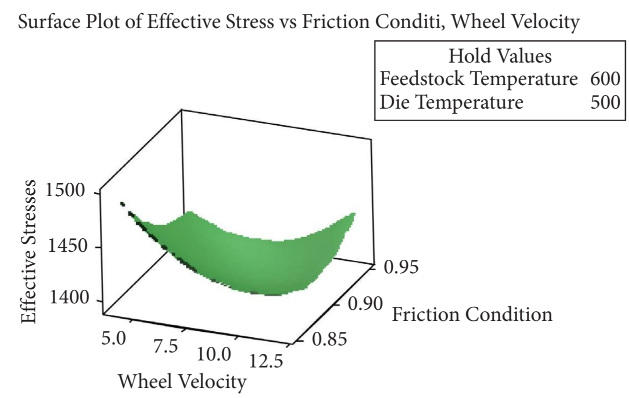

FIGURE 31: Surface graph occurred within effective stress vs. velocity of wheel and friction factor.

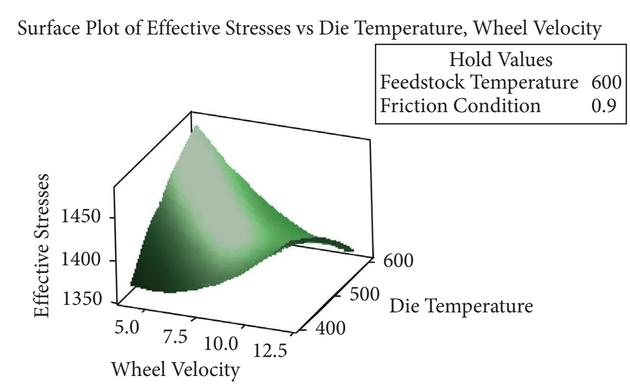

FIGURE 32: Surface graph occurred within effective stress vs. speed of wheel and die temperature.

The effect of wheel velocity and friction factor on effective stress is also supposed from Figure 25. The stress induced in the alloy due to the entire CEP extrusion is largest in the dark green zone; however, it is the least the light green zone. As a result, it is possible to deduce which the least effective stress induced in the alloy which is lower than 1400 N/mm^2 if the wheel velocity was between 6 and 10.5 rpm and friction factors are just above 0.887 taking holding values of feedstock temperature at 600°C and die temperature at 500°C.

An influence of wheel speed and temperature of die on effective stress can be observed in Figure 26. The effective stress induced in the alloy is greatest within the dark green zone and least inside the light green zone in the dark blue one. So, it is possible to conclude from the figure that the least effective stress that is lower than 1360 N/mm^2 if both the wheel velocity and die temperature are very high by taking holding values of feedstock temperature at 600°C and friction factor at 0.9.

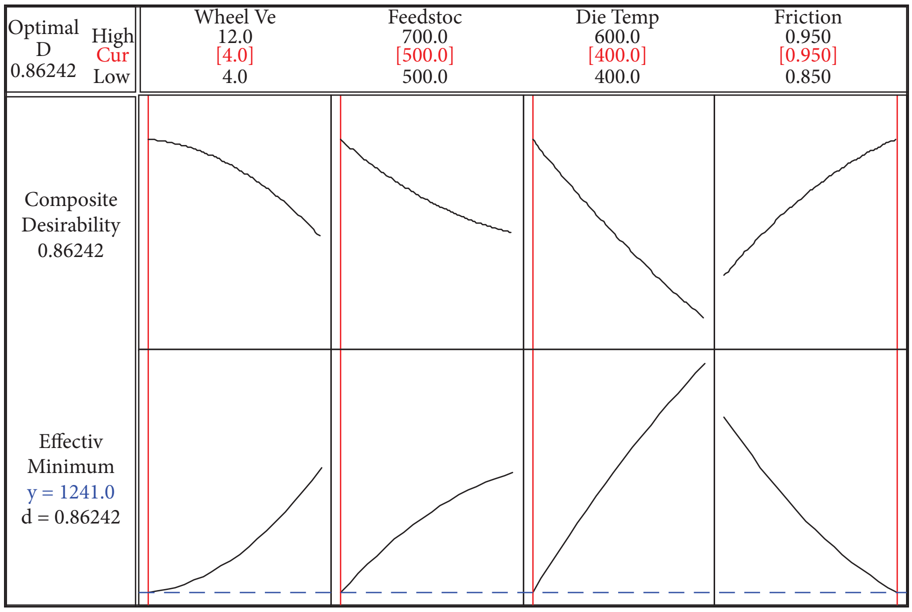

Figure 33: Optimization of the effective stress effect via speed of wheel, temperature of feedstock, temperature of die, and factor of friction.

Figure 27 shows a saddle-shaped effective stress 3D surface plot for wheel speed and feedstock temperature. The lowest stress was induced when FT was well below 530°C and WV between 8 and 11 rpm at holding values of 500°C FT and 0.9FF.

Figure 28 shows a 3D surface plot of effective stress for friction factor and die temperature. It became the lowest if the former variable is very high and the latter one is very low.

Figure 29 shows a flattened and twisted saddle-shaped 3D surface plot for effective stress for friction factor and feedstock temperature. It became the lowest if the friction factor was very high and feedstock temperature is very low simultaneously.

Figure 30 shows effective stress surface plot for die temperature and feedstock temperature. It became the lowest if both the CE input parameters are of very low levels.

Figure 31 shows a bowl-shaped effective stress 3D surface plot for wheel velocity and friction factor. It became the lowest if both the input parameters are in the middle.

Figure 32 shows a saddle-shaped effective stress surface plot for wheel velocity and die temperature. It became the lowest if both the input parameters are either in the lowest or highest levels simultaneously.

It has been seen from Figure 33 that although the minimum effective stress of 1241.0 was induced in the alloy due to the continuous forming process if the wheel velocity, feedstock temperature, die temperature, and frictional factor situations are 4 rpm, 500°C, 400°C, and 0.95, respectively. The optimum value of effective stress 1241.0 RSM yielded a composite desirability/worthiness of 1.0.

4. Conclusions

A numerical simulation of a copper alloy (C18150) material of feedstock at several feedstock and die temperatures, velocities of wheel, and factors of friction has been performed with the aid and assistance of a simulation software DEFORM-3D in the manuscript. A mathematical model based on RSM has been developed to investigate the effect velocity of wheel, die and feedstock temperatures, and factors of friction happening for the optimized total load needed for material of feedstock deformation and extrusion and the minimum effective stresses induced due to the processes. The optimal load of 408.167 kN is needed uncertainty the velocity of wheel, temperature of feedstock, die temperature, and factors of frictional circumstance are 4 rpm, 700°C, 600°C, and 0.85, respectively. Utilizing RSM, the optimal load/pressure is acquired with a composite favorability of 1.0. The minimum effective stress of 1241.0 MPa is induced due to the process if the velocity of wheel, temperature of feedstock, die temperature, and factors frictional situation were 4 rpm, 500°C, 400°C, and 0.95, respectively. The optimum value of effective stress 1241.0 MPa is RSM which yielded a composite preference/worthiness of 1.0. The presented research work is expected to assist industry sectors and various firms and researchers working in the development fields the continuous forming process leading towards the increased tooling's life and minimum power consumption.

Data Availability

The datasets used and/or analyzed during the current study are available from the corresponding author upon reasonable request.

Conflicts of Interest

The authors declare that they have no conflicts of interest.

Authors' Contributions

Tariku Desta carried out investigation of the study and wrote the original draft. Devendra Kumar Sinha performed writing, review, and editing. Perumalla Janaki Ramulu conducted supervision.

Acknowledgments

The authors would like to acknowledge Adama Science and Technology University and the Ministry of Education for their vital economic facticity contribution to this research work.

References

[1] D. Green, "Continuous extrusion of wire sections," *Journal of the Institute of Metals*, vol. 100, pp. 296–300, 1972.
[2] M. Bride water and B. Maddock, "New developments in conform Technology for continuous extrusion," *Proceedings of the 5th International Aluminium Extrusion Technology Seminar*, pp. 413–419, Aluminium Extruders Council and the Aluminium Association, Chicago, IL, USA, 1972.
[3] Y. H. Kim, J. R. Cho, H. Jeong, K. Kim, and S. S. Yoon, "A study on optimal design for CONFORM process," *Journal of Materials Processing Technology*, vol. 80-81, pp. 671–675, 1998.
[4] Y. Kim, J. Cho, K. S. Kim, H. S. Jeong, and S. S. Yoon, "A study of the application of upper bound method to the CONFORM process," *Journal of Materials Processing Technology*, vol. 97, no. 1-3, pp. 153–157, 2000.
[5] T. Manninen, T. Katajarinne, and P. Ramsay, "Analysis of Flash formation in continuous rotary extrusion of copper," *Journal of Materials Processing Technology*, vol. 177, no. 1-3, pp. 600–603, 2006.
[6] T. Katajarinne, T. Manninen, and P. Ramsay, "Numerical simulation of Flash formation in continuous rotary extrusion of copper," *Journal of Materials Processing Technology*, vol. 177, no. 1-3, pp. 604–607, 2006.
[7] J. Lu, N. Saluja, A. Riviere, and Y. Zhou, "Computer modeling of the continuous forming extrusion process of AA6061 alloy," *Journal of Materials Processing Technology*, vol. 79, no. 1-3, pp. 200–212, 1998.
[8] K. Khawaja, L. Seneviratne, and M. Clode, "Benefits of wheel-tool gap sensing in Conform™ extrusion machinery," *IEEE*, vol. 10, no. 4, pp. 428–436, 2005.
[9] K. Khawaja and L. Seneviratne, "Sensing & control of Conform™ extrusion gap between wheel and tooling plates," in *Proceedings of the ASME International Conference on Advanced Intelligent Mechatronics*, vol. 1, pp. 8–12, Seattle, WA, USA, June 2001.
[10] K. Khawaja, M. P. Clode, K. Althoefer, and L. Seneviratne, "Gap sensing benefits in Conform™ extrusion machinery," in *Proceedings of the International Conference on Robotics and Automation*, Yokohama, Japan, May 2004.
[11] J. R. Cho and H. S. Jeong, "Parametric investigation on the surface defect occurrence in CONFORM process by the finite element method," *Journal of Materials Processing Technology*, vol. 104, no. 3, pp. 236–243, 2000.
[12] Z. Jurkovic, M. Jurkovic, and S. Buljan, "Optimization of extrusion force prediction model using different techniques," *Journal of Achievements in materials and manufacturing engineering*, vol. 17, no. 1-2, pp. 353–357, 2006.
[13] J. R. Cho and H. S. Jeong, "CONFORM process: surface separation, curling and process characteristics to the wheel diameter," *Journal of Materials Processing Technology*, vol. 136, no. 1-3, pp. 217–226, 2003.
[14] P. Wu, S. Xie, H. Li, M. Yan, G. Huang, and L. Cheng, "Effect of extrusion wheel angular velocity on continuous extrusion forming process of copper concave bus bar," *Transactions of Nonferrous Metals Society of China*, vol. 17, no. 2, pp. 280–286, 2007.
[15] Y. Zhao, B. Song, J. Pei, C. Jia, B. Li, and G. Linlin, "Effect of deformation speed on the microstructure and mechanical properties of AA6063 during continuous extrusion process," *Journal of Materials Processing Technology*, vol. 213, no. 11, pp. 1855–1863, 2013.
[16] D. K. Sinha and S. Kumar, *Effect of Feedstock Temperature in Continuous Extrusion*, AIMTDR, Guwahati, India, 2014.
[17] T. Desta, D. K. Sinha, P. J. Ramulu, and H. B. Tufa, "Microstructural and mechanical studies of feedstock material in the continuous extrusion process," *International Journal of Mechanical and Materials Engineering*, vol. 16, no. 1, pp. 1–14, 2021.
[18] D. K. Sinha, S. Kumar, A. Kumar, and A. Yadav, "Optimization of process parameters in continuous extrusion of Aluminum alloy," in *Proceedings of the International Conference on Computational and Characterization Techniques in Engineering and Science (CCTES)*, Lucknow, India, September 2018.
[19] J. Hodek and M. Zemko, "FEM model of continuous extrusion of titanium in Deform software," *COM*, vol. 11, pp. 21-22, 2012.
[20] J. Hodek, T. Kubina, and J. Dlouhy, *FEM model of continuous extrusion of titanium in Deform software METAL*, Springer, Berlin, Germany, 2013.
[21] M. Zemko, J. Hodek, L. Kraus, and J. Dlouhy, "FEM modelling of continuous extrusion of high-strength metals using commercial Conform™ machine," *Advanced Science Letters*, vol. 19, no. 3, pp. 701–704, 2013.
[22] T. Desta, D. K. Sinha, P. J. Ramulu, and R. S. Singh, "Numerical modeling and optimization of process parameters in continuous extrusion process through response surface methodology, artificial neural network & genetic algorithm," *International Journal of Modeling, Simulation, and Scientific Computing*, vol. 12, no. 6, Article ID 2150060, 2021.
[23] M. R. Phate, S. B. Toney, and V. R. Phate, "Multi-parametric optimization of WEDM using artificial neural network (ANN)-Based PCA for Al/SiCp MMC," *J. Inst. Eng. India Ser. C*, vol. 102, no. 1, pp. 169–181, 2020.
[24] J. Wang and W. Wan, "Optimization of fermentative hydrogen production process using genetic algorithm based on neural network and response surface methodology," *International Journal of Hydrogen Energy*, vol. 34, no. 1, pp. 255–261, 2009.
[25] Z. Ding, S. Jia, P. Zhao, M. Deng, and K. Song, "Hot deformation behavior of Cu–0.6 Cr–0.03 Zr alloy during compression at elevated temperatures," *Materials Science and Engineering A*, vol. 570, pp. 87–91, 2013.
[26] Y. Nomura, R. Suzuki, and M. Saito, "Strength of copper alloys in high temperature environment," *Journal of Nuclear Materials*, vol. 307–311, pp. 681–685, 2002.
[27] Y. Zhang, Z. Chai, A. A. Volinsky et al., "Processing maps for the Cu-Cr-Zr-Y alloy hot deformation behavior," *Materials Science and Engineering A*, vol. 662, pp. 320–329, 2016.
[28] Y. Zhang, H. L. Sun, A. A. Volinsky et al., "Characterization of the hot deformation behavior of Cu–Cr–Zr alloy by processing maps," *Acta Metallurgica Sinica*, vol. 29, no. 5, pp. 422–430, 2016.
[29] A. Sarkar, M. J. N. V. Prasad, and S. N. Murty, "Effect of initial grain size on hot deformation behaviour of Cu-Cr-Zr-Ti alloy," *Materials Characterization*, vol. 160, Article ID 110112, 2020.
[30] A. Sarkar, S. N. Murty, and M. J. N. V. Prasad, "Effect of deformation mode on hot deformation characteristics and

microstructural evolution in Cu-Cr-Zr-Ti alloy," *Materials Characterization*, vol. 186, Article ID 111813, 2022.

[31] P. Aveiro, *Design of Experiments in Production Engineering*, J. P. Davim, Ed., Springer International Publishing, New York, NY, USA, 2016.

[32] J. P. Davim, *Statistical and Computational Techniques in Manufacturing*, Springer Science & Business Media, Singapore, 2012.

[33] U. S. Dixit, S. N. Joshi, and J. P. Davim, "Incorporation of material behavior in modeling of metal forming and machining processes: a review," *Materials and Design*, vol. 32, no. 7, pp. 3655–3670, 2011.

[34] V. A. Pandya and P. M. George, "Effect of preform design on forging load and effective stress during closed die hot forging process of pin," *Materials Today: Proceedings*, vol. 44, pp. 106–112, 2021.